EPTT 2024
Escola de Primavera de Transição e Turbulência

ABCM
Associação Brasileira de Engenharia e Ciências Mecânicas

INVESTIGATION OF FINITE WING EFFECTS IN TRANSITIONAL AIRFOIL FLOWS USING THE LATTICE-BOLTZMANN METHOD

Bernardo Luiz R. Ribeiro*
Cayan A. Dantas†
William R. Wolf‡
University of Campinas, Campinas, SP, Brazil, 13083-860
beluiz@unicamp.br*
c253092@dac.unicamp.br†
wolf@fem.unicamp.br‡

Abstract. *This study evaluates the ability of a lattice-Boltzmann high-fidelity simulation tool to resolve transitional flows with intermittent events. Here, the lattice-Boltzmann method (LBM) is employed to investigate the flow over a NACA0012 airfoil at an angle of attack of* $\boldsymbol{\alpha = 3°}$*, freestream Mach number* $\boldsymbol{M_\infty = 0.3}$*, and Reynolds number* $\boldsymbol{Re = 5 \times 10^4}$*. This flow configuration is typically found in the development of quiet air vehicles, making the study of noise generation mechanisms particularly relevant. For this case, a laminar separation bubble forms on the airfoil's suction side, leading to complex dynamics that include the shedding of coherent structures and the generation of trailing-edge tonal noise. Finite wing effects on the coherent structures are investigated and compared to the flow fields of a wing with periodic boundary conditions. The results indicate that the laminar separation bubble (LSB) on the suction side is significantly influenced by wing tip effects, forming much closer to the trailing edge than in the periodic wing. Additionally, an analysis of the vortex dynamics reveals distinct patterns of vortex shedding from the LSB, differing markedly from those observed in the spanwise homogeneous case. Overall, the finite wing impacts the pressure gradient along the wing, delaying the bubble formation and its subsequent vortex shedding and, hence, changing the acoustic noise generation.*

Keywords: *Lattice-Boltzmann, transitional flow, laminar separation bubble*

1. INTRODUCTION

The analysis of noise generation mechanisms in airfoils has been key to the development of quieter air vehicles. To this end, flows at various Reynolds numbers, including laminar, transitional, and turbulent regimes, as well as different airfoils and angles of attack, have been extensively investigated in the literature (Paterson *et al.*, 1972; Arbey and Bataille, 1983; Brooks *et al.*, 1989; Moreau *et al.*, 2011; Wolf *et al.*, 2012; Pröbsting *et al.*, 2015; Ricciardi and Wolf, 2022; Sano *et al.*, 2023). In this work, we perform 3D numerical simulations of two flow configurations. One configuration, following the work of Ricciardi *et al.* (2022), involves a spanwise periodic flow over a NACA0012 airfoil. The other configuration involves a flow over a finite wing with the same NACA0012 profile, where tip effects are considered on the formation of coherent structures over the foil. For both cases, the Reynolds and Mach numbers are $Re = 5 \times 10^4$ and $M_\infty = 0.3$, respectively, and the angle of attack is set as $\alpha = 3°$.

Depending on the Reynolds number, different mechanisms drive the acoustic noise generation. At low to moderate values ($Re < 10^5$), flow events over the foil's suction side dominate over those on the pressure side, whereas at high values, the opposite is true (Pröbsting *et al.*, 2015; Ricciardi and Wolf, 2022). A major feature of low Reynolds number flows is the formation of a laminar separation bubble (LSB) on the airfoil's suction side. This bubble exhibits intermittent behavior that modulates the shedding of coherent structures advected towards the trailing edge (TE) (Ricciardi *et al.*, 2020). Pröbsting and Yarusevych (2015) showed that a NACA0012 airfoil at Reynolds numbers 0.65 x $10^5 \leq Re \leq 4.5$ x 10^5 and $\alpha = 2°$ presents intermittent laminar–turbulent transition, affecting the convection of coherent structures from the LSB over the suction side towards the TE. In this case, the scattering of these spanwise-coherent structures is a major mechanism for airfoil noise generation.

In this work, we address the finite wing effects on the LSB formation and the laminar-turbulent transition over the wing. This analysis is important when investigating wing configurations of small air vehicles. In applications involving vertical take-off and landing (VTOL) configurations, the blades are in a rotational motion and the tip vortices from one

blade influence the flow over the adjacent one (Gourdain *et al.*, 2018; Vittal-Shenoy, 2023). The tip vortices shed from the blade influence the LSB formation, which is a key factor in the noise generation mechanisms from trailing edges (Gourdain *et al.*, 2017). Using numerical simulations, Vittal-Shenoy investigated the noise sources of a rotating blade and found that increasing the Mach number at the blade tip causes the LSB to separate earlier, delaying reattachment (Vittal-Shenoy, 2023).

The objective of this paper is to assess the capability of the lattice-Boltzmann method (LBM) in resolving a transitional airfoil flow over a finite wing (without rotation effects). This analysis is performed through 3D numerical simulations run in direct numerical simulation (DNS) mode, i.e., without subgrid scale or wall models available in the present LBM solver. Due to its simpler partial differential equation system compared to traditional Navier-Stokes solvers, the LBM offers advantages in terms of simulation time and scalability (Moreau *et al.*, 2011). Furthermore, the results are compared to a LBM case where periodic boundary conditions are applied, following the flow configuration from Ricciardi and Wolf (2022) where they used wall-resolved large eddy simulation (LES) to solve the Navier-Stokes equations.

2. METHODOLOGY

2.1 Numerical Simulations

2.1.1 Lattice-Boltzmann solver

Numerical simulations are conducted using the commercial code SIMULIA PowerFLOW 6-2022, a high-fidelity LBM-based software. The LBM resolves fluid flows at the mesoscopic scale in a statistical sense, having origin in the lattice gas models (Krüger *et al.*, 2017). While these models track the behavior of particles at a microscopic scale, the LBM instead tracks the advection and collision of fluid particles using discrete distribution functions $f_i(\boldsymbol{x}, t)$, often called particle populations (Teruna *et al.*, 2020). The term f_i represents the density of particles travelling with velocity $\boldsymbol{c} = (c_x, c_y, c_z)$ from the position $\boldsymbol{x} = (x, y, z)$ at a time t in the direction i. The velocity is chosen so that particles travel one cell per timestep, effectively making the Courant–Friedrichs–Lewy (CFL) number for f_i equal to one Ribeiro *et al.* (2016). The LBM equation (Chen *et al.*, 1997) is written as

$$f_i(\boldsymbol{x} + \boldsymbol{c}_i\Delta t, t + \Delta t) - f_i(\boldsymbol{x}, t) = \Omega_i(\boldsymbol{x}, t)\,, \tag{1}$$

where Ω_i represents the collision operator and Δt is the timestep. The left-hand side of Eq. (1) represents particles moving with velocity $\boldsymbol{c}$ in the i-th direction to a neighbouring point $\boldsymbol{x} + \boldsymbol{c}_i\Delta t$ at the next timestep $t + \Delta t$. On the right-hand side, particle collisions are modeled by redistributing them among f_i at each site. In PowerFLOW, the collision term is modeled using the approximation described by Bhatnagar *et al.* (1954) as

$$\Omega_i(\boldsymbol{x}, t) = -\frac{\Delta t}{\tau}[f_i(\boldsymbol{x}, t) - f_i^{eq}(\boldsymbol{x}, t)]\,, \tag{2}$$

where τ is the relaxation time, which is related to the non-dimensional fluid viscosity ν through the relation $\nu = c_s^2(\tau - \Delta t/2)$ (Ribeiro *et al.*, 2018). Here, c_s is the non-dimensional speed of sound, and the term f_i^{eq} is the equilibrium Maxwell-Boltzmann distribution function, which is approximated by a second-order expansion (Chen *et al.*, 1992) as

$$f_i^{eq} = w_i\rho\left(1 + \frac{\boldsymbol{c}_i \cdot \boldsymbol{u}}{c_s^2} + \frac{(\boldsymbol{c}_i \cdot \boldsymbol{u})^2}{2c_s^4} - \frac{\boldsymbol{u} \cdot \boldsymbol{u}}{2c_s^2}\right)\,, \tag{3}$$

where w_i represents weighting coefficients which depend on the direction being calculated, while ρ is the fluid density and $\boldsymbol{u}$ is the fluid velocity. Together with a corresponding set of w_i, $\boldsymbol{c}_i$ forms velocity sets usually denoted by DdQq, where d is the number of spatial dimensions of the velocity set, and q represents the number of discrete velocity directions. In PowerFLOW, the D3Q19 velocity set is used for three-dimensional flows (Himeno *et al.*, 2021).

The phenomenon of transition to turbulence requires a level of spatial and temporal resolution that is compatible with direct numerical simulation (DNS) or wall-resolved large eddy simulation (LES). The turbulence modeling capability of PowerFLOW (Chen *et al.*, 2003), which enables a numerical procedure called very large eddy simulation (VLES), has not been shown to capture laminar-turbulence transition yet. Therefore, in the present work we perform simulations in the DNS mode, i.e., we do not employ subgrid or wall models available in the solver.

The link between Eq. (1) and the Navier-Stokes (NS) equations can be determined using the Chapman-Enskog analysis (Chapman *et al.*, 1990). Once f_i is known, macroscopic flow variables, such as ρ and $\boldsymbol{u}$ are obtained by taking the zeroth- and first-order moments of f_i (Souza *et al.*, 2019), respectively:

$$\rho(\boldsymbol{x}, t) = \sum_{i=0}^{q-1} f_i(\boldsymbol{x}, t)\,, \tag{4}$$

and

$$\rho(\boldsymbol{x},t)\boldsymbol{u}(\boldsymbol{x},t) = \sum_{i=0}^{q-1} \boldsymbol{c}_i f_i(\boldsymbol{x},t)\ . \tag{5}$$

The LBM is solved on a lattice composed of cubic volumetric elements called voxels. The simulation domain can be subdivided into several regions where different voxel resolutions are applied (Teruna *et al.*, 2021), such that the resolution between two adjacent regions varies by a factor of 2. Solid boundaries are discretized using computational surface elements (surfels) that are generated at locations where the voxels intersect solid surfaces (facets) (Chen *et al.*, 1998). The process of generating voxels and surfels is fully automated. The boundary condition at a solid wall is computed by applying appropriate particle interactions in the collision term of the LBM. PowerFLOW results are transient and time accurate, where the time advancement is performed by an explicit scheme which allows for efficient and highly-scalable simulations.

2.2 Flow configuration and mesh details

The flow configuration of interest corresponds to a NACA0012 airfoil with a rounded trailing edge at a Reynolds number $Re = 5 \times 10^4$, a freestream Mach number of $M_\infty = 0.3$, and an angle of attack of 3°. The simulation domain is cubical with 60 chord lengths in size, where a finite wing with a span of one chord length is placed at the center of the domain. All domain surfaces are defined as a flow outlet boundary condition, except for the surface closest to the leading edge and perpendicular to the foil chord which is defined as an inlet. A no-slip boundary condition is specified at the airfoil surface and no wall modeling is used in the present study in order to precisely capture the laminar to turbulent transition of the boundary layer. The simulations run for $7.7 \times 10^{-2} s$ of physical time, using AMD EPYC 7443 processors. The parallel simulations employed 1008 cores for 288 hours in wall-clock time, which is equivalent to approximately 2.9×10^5 CPU hours.

The mesh is composed of voxels whose sizes are controlled by 16 variable resolution (VR) regions. The finest voxels of the mesh are located on the airfoil surface and their size consist of 0.0197% of the chord. This number leads to 5078 voxels across the spanwise and streamwise directions in the finest VR. The voxel size is increased by a factor of 2 from one VR region to another, ensuring a proper flux discretization at the interfaces. The first three finest VR regions are applied as an offset of the NACA0012 profile, while the other 13 VRs are boxes enclosing the airfoil. The mesh is constructed so that the boundary layer fits inside the two finest regions, resulting in a total of 2 billion voxels in the mesh.

3. RESULTS

The results are divided in two parts, being the mean flow and vortex dynamics analyses.

3.1 Mean flow analysis

First, we analyze the mean flow LBM solutions in terms of the LSB size and location. For this purpose, the streamwise velocity and root-mean-square (RMS) of the turbulent kinetic energy, k, are compared against the periodic wing configuration, where periodic boundary conditions are used. In Figs. 1a and 1b, the time- and spanwise-averaged streamwise velocity and RMS of k from a wing with periodic boundary conditions are displayed for purposes of comparison. For the finite wing, two slices are considered: one placed at midspan (Figs. 1c and 1d) and the other near the tip (Figs. 1e and 1f). A magenta line depicting the reversed flow region is included in each subfigure.

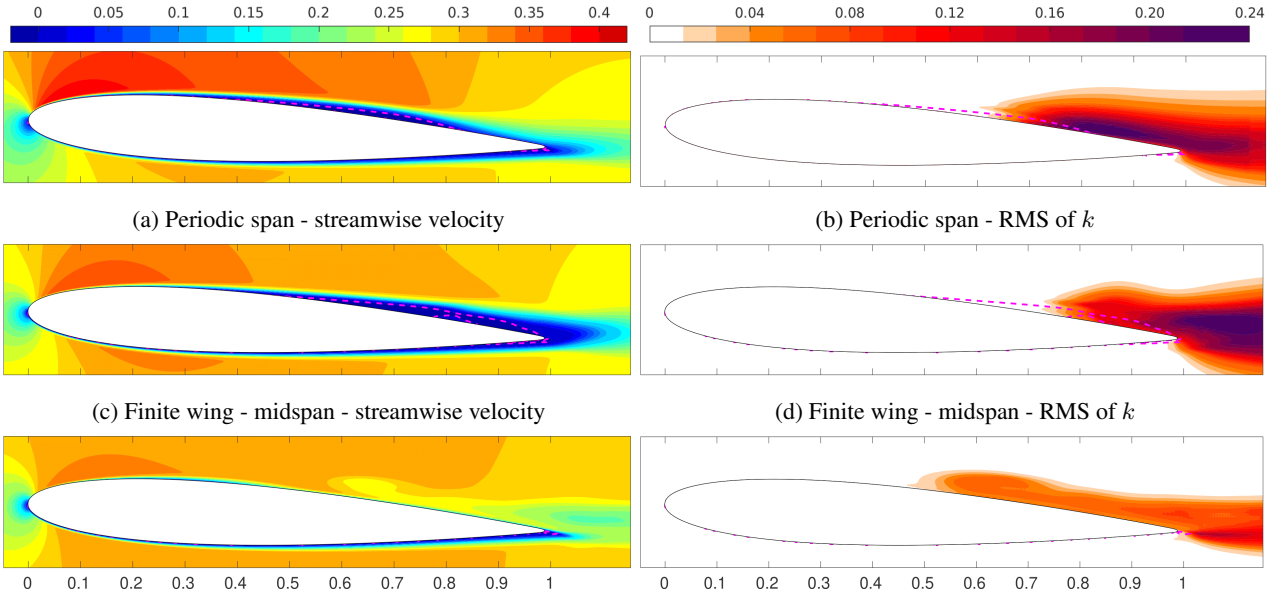

(a) Periodic span - streamwise velocity

(b) Periodic span - RMS of k

(c) Finite wing - midspan - streamwise velocity

(d) Finite wing - midspan - RMS of k

(e) Finite wing - tip location - streamwise velocity

(f) Finite wing - tip location - RMS of k

Figure 1: Time-averaged flow fields of the streamwise velocity (left column) and RMS of k (right column), for a wing with spanwise periodic boundary conditions compared with the flow fields at midspan and tip of a finite wing.

Comparing the flow fields at the midspan of the finite wing with those from the periodic wing, one can notice that the LSB forms closer to the trailing edge in the former configuration. Moreover, the bubble is thicker at midspan for the finite wing case, and appears to merge with the wake. Higher values of streamwise velocity are observed in the wing with spanwise periodic boundary conditions. This is due to the flow confinement effect that occurs in this configuration. High values of the RMS of k are located near the reattachment point for the periodic wing, as shown in Fig. 1b, while the most prominent values of k are observed at the trailing edge and in the wake, at the midspan of the finite wing. In contrast, the streamwise velocity field near the tip does not display any flow separation, and thus a LSB is not formed. This is due to a relaminarization caused by the wing tip on the suction side, which prevents the flow from separating. The values of RMS of k are considerably smaller near the wing tip, and appear downstream the mid-chord and in the wake.

To gain a better understanding of the reattachment process, a view from the trailing edge is displayed in Fig. 2. The slice location is at approximately 90% of the chord. In the periodic span configuration, the slice does not display a reversed flow since the LSB reattaches further upstream on the suction side. For this case, the bubble ranges from $x/c \approx 0.3$ to 0.8. In contrast, a recirculation region is observed around the midspan in the finite wing configuration. However, as the one approaches the tip, the recirculation zone is damped due to the tip vortices that inject momentum over the wing through a downwash effect that in turn keeps the flow attached to the foil. In the same figure, the RMS of k is also presented for both airfoils. A uniform distribution of turbulent kinetic energy is observed for the periodic span case, depicting that the velocity fluctuations are strong near the trailing edge. On the other hand, lower values of k are shown for the finite wing. These values are concentrated around the midspan, where the separation bubble is formed (delimited by dashed magenta line), and along the wing extremities, where the tip vortices induce velocity fluctuations. Between the wing tips and the midspan, velocity fluctuations are not observed, indicating that the flow is laminar and steady.

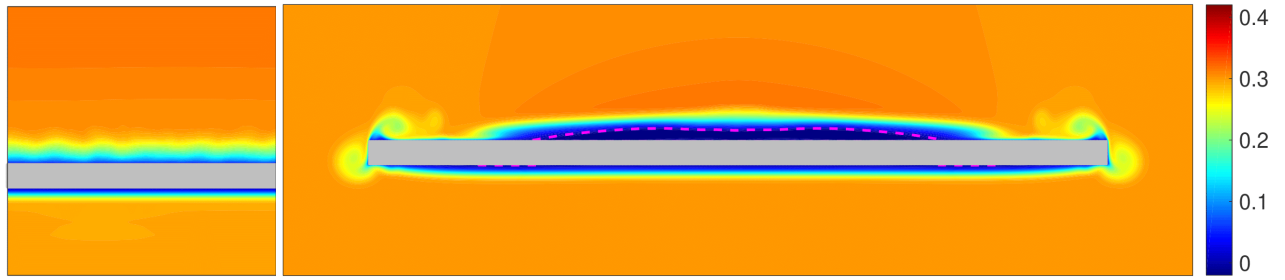

(a) Periodic span (b) Finite wing - Streamwise velocity

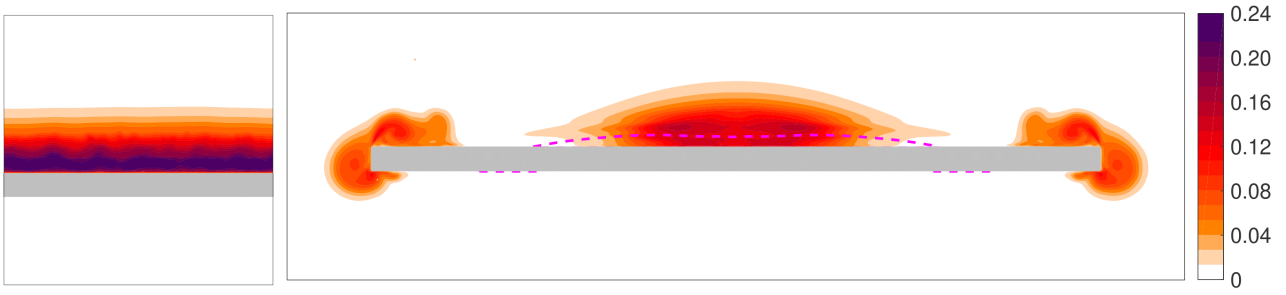

(c) Periodic span (d) Finite wing - RMS of k

Figure 2: Time-averaged flow fields of the streamwise velocity and RMS of k near the trailing edge on a wing with spanwise periodic boundary conditions (left column) compared with the flow fields of a finite wing (right column). A constant x-slice is taken at the same locations on both wings to display a view from the trailing edge.

3.2 Vortex dynamics analysis

The effects of flow restriction in the spanwise direction can be visualized through isosurfaces of λ_2 colored by the streamwise velocity in Fig. 3. Both the perspective and top (suction side) views of the finite and periodic wings are displayed. The isosurfaces of λ_2 over the suction side of the finite wing depict vortical structures forming near the trailing edge, which is demarked by a black line in all subplots. These structures are coherent along a small portion of the span. At the wing tips, one can see the turbulent structures formed around the tip vortices, which grow in size along the chord, towards the central portion of the wing. In the wake, the flow is turbulent but still shows some organized motion from the midspan region. In contrast, the isosurfaces of λ_2 on the periodic wing display spanwise coherent structures forming upstream, near the reattachment location. For the instant presented in the figure, one can see that the structures remain coherent as they are advected towards the trailing edge and the wake. The structures formed over the finite wing arise due to a shear layer instability near the bubble close to the trailing edge. They differ in shape compared to the structures shed from the LSB of the periodic case.

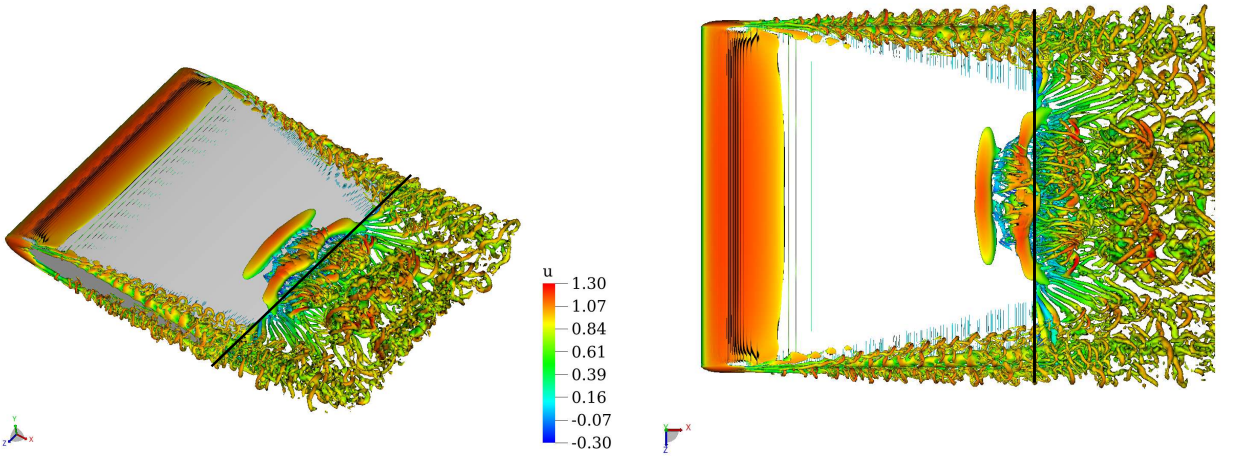

(a) Finite wing - perspective view

(b) Finite wing - top view

(c) Periodic span - perspective view

(d) Periodic span - top view

Figure 3: Instantaneous isosurfaces of λ_2 colored by u-velocity component (streamwise direction) for the finite wing and the spanwise periodic wing. For an easier visualization of the structures shed over the suction side of the wings, both perspective and top views are presented. The black line in each figure indicates the trailing edge location.

4. CONCLUSIONS

We conducted an assessment of the LBM for solving a transitional airfoil flow. Results are compared between a wing with periodic boundary conditions and a finite wing. The numerical simulations are performed for a NACA0012 airfoil with Reynolds number $Re = 5 \times 10^4$, freestream Mach number of $M_\infty = 0.3$, and angle of attack $\alpha = 3°$. The objective of this work is to analyze finite wing effects on the present transitional flow and compare the solution to a periodic wing setup. We are particularly interested in studying the mean flow differences induced by the finite wing, including the effects of tip vortices, the LSB dynamics and the structures shed by the bubble, besides their subsequent aeroacoustic trailing-edge noise generation.

We show that the finite wing effects lead to a reattachment of the flow over the wing suction side, causing changes in the pressure distribution and friction coefficient. From the latter, we observe that the separation bubble of the finite wing is displaced downstream towards the trailing edge, being three-dimensional due to wing tip effects. The physics of vortex formation and shedding is considerably different when compared to the periodic wing configuration. This study highlights important aspects to consider when investigating the unsteady aerodynamics and aeroacoustics of finite aspect ratio wings.

5. ACKNOWLEDGEMENTS

The authors thank CENAPAD-SP (Project 551 - Cluster Lovelace) for providing the computational resources used in this study. We acknowledge Fundação de Amparo à Pesquisa do Estado de São Paulo (FAPESP) for supporting the present work under research grants No. 2013/08293-7, 2021/06448-0 and 2023/08768-7. We also acknowledge a scholarship to the first author funded by Coordenação de Aperfeiçoamento de Pessoal de Nível Superior, CAPES, under

grant 88887.825328/2023-00.

6. REFERENCES

Arbey, H. and Bataille, J., 1983. "Noise generated by airfoil profiles placed in a uniform laminar flow". *Journal of Fluid Mechanics*, Vol. 134, pp. 33–47. ISSN 1469-7645. doi:10.1017/S0022112083003201.

Bhatnagar, P.L., Gross, E.P. and Krook, M., 1954. "A model for collision processes in gases. i. small amplitude processes in charged and neutral one-component systems". *Physical Review*, Vol. 94, pp. 511–525. doi:10.1103/PhysRev.94.511.

Brooks, T.F., Pope, D.S. and Marcolini, M.A., 1989. "Airfoil self-noise and prediction". Technical report, NASA.

Chapman, S., Cowling, T.G. and Park, D., 1990. "The mathematical theory of non-uniform gases". Cambridge University Press. doi:https://doi.org/10.2307/3607024.

Chen, H., Chen, S. and Matthaeus, W.H., 1992. "Recovery of the navier-stokes equations using a lattice-gas boltzmann method". *Physical Review*, Vol. 45, pp. R5339–R5342. doi:10.1103/PhysRevA.45.R5339.

Chen, H., Kandasamy, S., Orszag, S., Shock, R., Succi, S. and Yakhot, V., 2003. "Extended boltzmann kinetic equation for turbulent flows". *Science*, Vol. 301, pp. 633–636. doi:https://doi.org/10.1126/science.1085048.

Chen, H., Teixeira, C. and Molvig, K., 1997. "Digital physics approach to computational fluid dynamics: Some basic theoretical features". *International Journal of Modern Physics C*, Vol. 8, p. 675–684. doi:10.1142/s0129183197000576.

Chen, H., Teixeira, C. and Molvig, K., 1998. "Realization of fluid boundary conditions via discrete boltzmann dynamics". *International Journal of Modern Physics C*, Vol. 9, pp. 1281–1292. doi:10.1142/s0129183198001151.

Gourdain, N., Jardin, T., Serre, R., Prothin, S. and Moschetta, J.M., 2018. "Application of a lattice Boltzmann method to some challenges related to micro-air vehicles". *International Journal of Micro Air Vehicles*, Vol. 10, No. 3, pp. 285–299. ISSN 1756-8293, 1756-8307. doi:10.1177/1756829318794174.

Gourdain, N., Singh, D., Jardin, T. and Prothin, S., 2017. "Analysis of the Turbulent Wake Generated by a Micro Air Vehicle Hovering near the Ground with a Lattice Boltzmann Method". *Journal of the American Helicopter Society*, Vol. 62, No. 4, pp. 1–12. ISSN 2161-6027. doi:10.4050/JAHS.62.042003.

Himeno, F.H., Souza, D.S., Amaral, F.R., Rodríguez, D. and Medeiros, M.A., 2021. "Spod analysis of noise-generating rossiter modes in a slat with and without a bulb seal". *Journal of Fluid Mechanics*, Vol. 915, No. A67. doi:10.1017/jfm.2021.93.

Krüger, T., Kusumaatmaja, H., Kuzmin, A., Shardt, O., Silva, G. and Viggen, E.M., 2017. *The Lattice-Boltzmann Method*, Vol. 10. Springer International Publishing. doi:https://doi.org/10.1007/978-3-319-44649-3.

Moreau, S., Sanjosé, M., Perot, F. and Kim, M.S., 2011. "Direct self-noise simulation of the installed Controlled Diffusion airfoil". In *17th AIAA/CEAS Aeroacoustics Conference (32nd AIAA Aeroacoustics Conference)*. American Institute of Aeronautics and Astronautics, Portland, Oregon. ISBN 978-1-60086-943-3. doi:10.2514/6.2011-2716.

Paterson, R.W., Vogt, P.G., Fink, M.R. and Munch, C.L., 1972. "Vortex noise of isolated airfoils". *Journal of Aircraft*, Vol. 10, pp. 296–302. doi:DOI:10.2514/3.60229.

Pröbsting, S., Scarano, F. and Morris, S.C., 2015. "Regimes of tonal noise on an airfoil at moderate Reynolds number". *Journal of Fluid Mechanics*, Vol. 780, pp. 407–438. ISSN 0022-1120, 1469-7645. doi:10.1017/jfm.2015.475.

Pröbsting, S. and Yarusevych, S., 2015. "Laminar separation bubble development on an airfoil emitting tonal noise". *Journal of Fluid Mechanics*, Vol. 780, pp. 167–191. ISSN 0022-1120, 1469-7645. doi:10.1017/jfm.2015.427.

Ribeiro, A., Fares, E. and Choudhari, M., 2018. "Dns of laminar to turbulent transition on naca 0012 airfoil with sand grain roughness". Technical report, NASA.

Ribeiro, A.F.P., Casalino, D., Fares, E. and Choudhari, M., 2016. "Direct numerical simulation of an airfoil with sand grain roughness on the leading edge". Technical report, NASA.

Ricciardi, T.R., Arias-Ramirez, W. and Wolf, W.R., 2020. "On secondary tones arising in trailing-edge noise at moderate Reynolds numbers". *Eur. J. Mech. B*, Vol. 79, pp. 54–66. ISSN 0997-7546.

Ricciardi, T.R. and Wolf, W.R., 2022. "Switch of tonal noise generation mechanisms in airfoil transitional flows". *Physical Review Fluids*, Vol. 7, No. 8, p. 084701. ISSN 2469-990X. doi:10.1103/PhysRevFluids.7.084701.

Ricciardi, T.R., Wolf, W.R. and Taira, K., 2022. "Transition, intermittency and phase interference effects in airfoil secondary tones and acoustic feedback loop". *Journal of Fluid Mechanics*, Vol. 937, p. A23. ISSN 0022-1120, 1469-7645. doi:10.1017/jfm.2022.129.

Sano, A., Cavalieri, A.V., da Silva, A.F. and Wolf, W.R., 2023. "On the emergence of secondary tones in airfoil noise". *Journal of Fluid Mechanics*, Vol. 966, p. A8. doi:10.1017/jfm.2023.442.

Souza, D.S., Rodríguez, D., Himeno, F.H.T. and Medeiros, M.A.F., 2019. "Dynamics of the large-scale structures and associated noise emission in airfoil slats". *Journal of Fluid Mechanics*, Vol. 875, p. 1004–1034. doi:10.1017/jfm.2019.496.

Teruna, C., Avallone, F., Ragni, D., Rubio-Carpio, A. and Casalino, D., 2021. "Numerical analysis of a 3-d printed porous trailing edge for broadband noise reduction". *Journal of Fluid Mechanics*, Vol. 926, No. A17. doi:10.1017/jfm.2021.704.

Teruna, C., Manegar, F., Avallone, F., Ragni, D., Casalino, D. and Carolus, T., 2020. "Noise reduction mechanisms of an open-cell metal-foam trailing edge". *Journal of Fluid Mechanics*, Vol. 898, No. A18. doi:10.1017/jfm.2020.363.

Vittal-Shenoy, D., 2023. *Aeroacoustic study of low Reynolds number rotors using Large Eddy Simulations*. Ph.D. thesis, l'Institut Supérieur de l'Aéronautique et de l'Espace (ISAE).

Wolf, W.R., Azevedo, J.L.F. and Lele, S.K., 2012. "Convective effects and the role of quadrupole sources for aerofoil aeroacoustics". *Journal of Fluid Mechanics*, Vol. 708, pp. 502–538. ISSN 0022-1120, 1469-7645. doi: 10.1017/jfm.2012.327.

7. RESPONSIBILITY NOTICE

The authors are the only responsible for the printed material included in this paper.